14. Yu. S. Kachanov, "Resonance wave nature of the transition to turbulence in a boundary layer," in: Modeling in Mechanics [in Russian], Vol. 1, No. 2 (1988).
15. V. N. Zhigulev and A. M. Tumin, Origin of Turbulence [in Russian], Nauka, Moscow (1987).

COMPUTING THE COMPRESSIBLE LAMINAR BOUNDARY LAYER ON A SHARP BODY OF BIELLIPTIC SECTION

V. N. Vetlutskii

UDC 532.526

The problem of determining the parameters of a three-dimensional boundary layer is very pertinent, since its solution gives the distribution of friction and heat flux at the surface of the immersed body. From numerical solution of the full boundary layer equations we find the flow parameters: velocity components, temperature and density, from which one obtains new knowledge of the whole flow picture.

Most papers on computing the laminar three-dimensional boundary layer deal with incompressible flow [1-5]. At supersonic speed of the incident flow it has been studied most frequently on blunt bodies (see, e.g., [6-9]). The three-dimensional compressible boundary layer on sharp bodies was examined in [10-13]. The angles of limiting stream lines computed in [10] and the velocity profiles on a circular cone at angle of attack were compared with experiment in [11]. The friction factor distributions were measured on ogive-cylindrical bodies in [12, 13].

The present paper describes a statement of the problem and computing algorithms for the compressible laminar boundary layer on a sharp body. Computed results are presented for a body of bielliptic cross section at Mach number $M_\infty = 2$ and angles of attack $\alpha = 0\text{-}10°$. The evolution of the three-dimensional boundary layer with variation of angle of attack is described.

1. We consider flow over a sharp body of fuselage shape, immersed in a supersonic stream of gas of Mach number M_∞. The body has a plane of symmetry, which contains the velocity vector of the incident flow. The vector makes the angle of attack α with a certain axis of the body. In this case the entire flow also has a plane of symmetry.

The body surface is assumed to be smooth, and its equation is given in a cylindrical coordinate system $r = r(\xi, \zeta)$. The coordinate ξ is reckoned from the body vertex along its axis, ζ is the meridional angle in the transverse section, and $\zeta = 0$ corresponds to the windward symmetry plane. The equations of the three-dimensional compressible laminar boundary layer have been written in the nonorthogonal coordinate system (ξ, η, ζ), fixed in the body surface [14]. The coordinate η coincides with the local surface normal.

The body nose is assumed to be conical. In that case the inviscid flow there is conical, and the boundary layer equations have a similarity solution dependent on the variables ζ, $\lambda = \eta/\sqrt{\xi}$ [15]. Therefore in this paper, in addition to the coordinate η we introduce the variable λ, and instead of the components of the velocity v directed along the normal to the body surface, we introduce the mass flux

$$j = \rho\left(v\sqrt{\xi} - u\eta/2\sqrt{g_{11}}\right).$$

Here and below g_{ik} are the metric coefficients of the surface. Of course, with this substitution we can avoid the solution depending on the longitudinal coordinate ξ only on the conical nose. On the rest of the surface the dependence of the boundary layer thickness on ξ in the new variable λ will be weaker.

We now write two equations of motion, the energy equation, and the continuity equation in the variables (ξ, λ, ζ) in the following form [16]:

Novosibirsk. Translated from Zhurnal Prikladnoi Mekhaniki i Tekhnicheskoi Fiziki, No. 1, pp. 55-61, January-February, 1991. Original article submitted May 19, 1989; revision submitted July 7, 1989.

0021-8944/91/3201-0051$12.50

$$\xi\frac{\rho u}{\sqrt{g_{11}}}\frac{\partial u}{\partial\xi}+\xi\frac{\rho w}{\sqrt{g_{22}}}\frac{\partial u}{\partial\zeta}+j\frac{\partial u}{\partial\lambda}-\frac{\partial}{\partial\lambda}\left(\mu\frac{\partial u}{\partial\lambda}\right)+P=0,\qquad(1)$$

$$\xi\frac{\rho u}{\sqrt{g_{11}}}\frac{\partial w}{\partial\xi}+\xi\frac{\rho w}{\sqrt{g_{22}}}\frac{\partial w}{\partial\zeta}+j\frac{\partial w}{\partial\lambda}-\frac{\partial}{\partial\lambda}\left(\mu\frac{\partial w}{\partial\lambda}\right)+Q=0,$$

$$c_p\left(\xi\frac{\rho u}{\sqrt{g_{11}}}\frac{\partial T}{\partial\xi}+\xi\frac{\rho w}{\sqrt{g_{22}}}\frac{\partial T}{\partial\zeta}+j\frac{\partial T}{\partial\lambda}\right)-\frac{1}{\mathrm{Pr}}\frac{\partial}{\partial\lambda}\left(k\frac{\partial T}{\partial\lambda}\right)-$$

$$-\xi c_{p_e}\left(\frac{\rho_e u_e}{\sqrt{g_{11}}}\frac{\partial T_e}{\partial\xi}+\frac{\rho_e v_e}{\sqrt{g_{22}}}\frac{\partial T_e}{\partial\zeta}\right)-(\gamma-1)\,\mathrm{M}_\infty^2\mu\left(\left(\frac{\partial u}{\partial\lambda}\right)^2+\right.$$

$$\left.+\left(\frac{\partial w}{\partial\lambda}\right)^2+2\frac{\partial u}{\partial\lambda}\frac{\partial w}{\partial\lambda}\frac{g_{12}}{g_{11}g_{22}}\right)=0,$$

$$\xi\left(\frac{\partial}{\partial\xi}\left(\rho u\sqrt{\frac{g}{g_{11}}}\right)+\frac{\partial}{\partial\zeta}\left(\rho w\sqrt{\frac{g}{g_{22}}}\right)\right)+\frac{\partial j}{\partial\lambda}\sqrt{g}+\frac{\rho u}{2}\sqrt{\frac{g}{g_{11}}}=0.$$

The equation of state $\rho = \gamma M_\infty^2 p/T$ closes the system. The functions P and Q depend on the components of velocity u and w in the boundary layer and at the outer edge. The remaining symbols are conventional. All the parameters are dimensionless relative to the body length X and their values in the incident flow. The pressure is referenced to twice the dynamic head.

In substituting the boundary conditions for the equations of the three-dimensional boundary layer one must be guided by a conception of zones of influence and dependence [17]. With its use the simple rule has been established: the velocity components and the temperature are given at two boundaries through which the fluid flows into the region examined, and conditions are not imposed on the remaining boundaries. This rule is based on proof of a uniqueness theorem for a model equation [18].

The main role in the three-dimensional boundary layer is played by the linear surfaces formed by normals to the flow surface and the containing stream lines. The velocity vectors coming from any generator of their normals lie in a single plane tangent to this linear surface. We shall call such a surface inflow if the stream lines come together at its surface, and outflow if the opposite is true.

The system of equations (1) was solved in the region $\Omega(\xi \geq \xi_0,\ 0 \leq \zeta \leq \zeta,\ 0 \leq \lambda \leq \lambda_e(\xi, \zeta))$ under the following boundary conditions:

$$\xi = \xi_0\colon\ u = u_0(\lambda,\ \zeta),\ w = w_0(\lambda,\ \zeta),\ T = T_0(\lambda,\ \zeta);$$

$$\zeta = 0\colon\ \partial u/\partial\zeta = 0,\ w = 0,\ \partial T/\partial\zeta = 0;$$

$$\lambda = 0\colon\ u = 0,\ w = 0,\ j = 0,\ T = T_w;$$

$$\lambda = \lambda_e(\xi,\ \zeta)\colon\ u = u_e(\xi,\ \zeta),\ w = w_e(\xi,\ \zeta),\ T = T_e(\xi,\ \zeta),\ p = p_e(\xi,\ \zeta).$$

Here the section $\xi = \xi_0$ corresponds to the conical body nose, and therefore the profiles of u_0, v_0, T_0 derive from the similarity solution. On the plane $\zeta = 0$ we assign the symmetry conditions in the case when it is an outflow surface, and we cannot assign conditions if the opposite is true. If the plane $\zeta = \zeta_+$ coincides with the plane of symmetry ($\zeta_+ = 180°$), then the situation with boundary conditions is similar to the plane $\zeta = 0$. The plane $\zeta = \zeta_+$ can be taken as not coinciding with the symmetry plane. There are no boundary conditions on it if the fluid flows through it.

On the body surface $\lambda = 0$ we assumed the usual conditions for a viscous fluid, i.e., no slip and impermeability, and equality of the gas and wall temperatures. At the outer edge of the boundary layer $\lambda = \lambda_e(\xi, \zeta)$ the flow parameters u_e, w_e, T_e, p_e are derived from computing flow of an inviscid gas over the given body.

2. On the conical nose the boundary layer problem has a similarity solution. The transformation of system (1) for this region was given in [16].

In this paper the body surface and the parameters at the outer edge were assigned in the form of two-dimensional tables. A spline interpolation of these data, and recomputation of the flow parameters to the coordinate system fixed in the body surface has also been described in [16]. The difference is that we used smoothing splines [19].

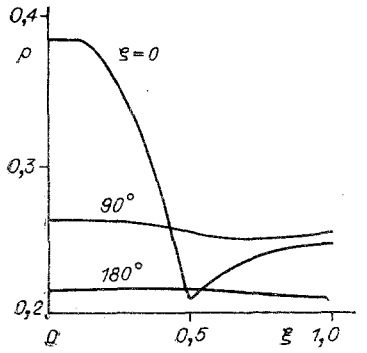

Fig. 1

In most three-dimensional boundary layer problems examined there is an outflow surface, which usually coincides with the plane of symmetry. The flow on the outflow surface is not described by the equations of the planar boundary layer, and depends on the second derivative of the pressure in the transverse direction [14]. However, the solution on this surface can be obtained independently of the solution in the remaining region.

The most widely used difference scheme for solving the three-dimensional boundary layer equations makes substantial use of the solution obtained on an outflow surface [1, 2, 20]. But the plane of symmetry can be an inflow surface, and the position of the outflow surface is not known beforehand. Then it is very difficult to use these schemes [21]. But if there is no outflow surface in the boundary layer, as is the case in a number of variants from [18] and in the present work, then these schemes are generally inapplicable.

We use a two-layer implicit difference scheme with weighting factors, described in detail in [4, 18]. With a value of weighting factor of $\theta = 0.5$ it is a second-order approximation in all the coordinates. In the example of a linear equation its absolute stability for $0.5 \leq \theta \leq 1.0$ was proved [18]. The advantage of this scheme is that we can include an outflow surface and it is fully applicable if the latter is not present.

This difference scheme was used with constant step size in each direction, and therefore to increase the computational accuracy we used stretching of coordinates fixed in the surrounding direction and automatically normal to the surface [16].

For a three-dimensional boundary layer there is great interest in the components of the friction stress c_{f_1}, c_{f_2} and the Stanton number on the body surface. The similarity coefficients $c_{f_1}{}^*$, $c_{f_2}{}^*$, St* were computed as follows:

$$c_{fi}^* = c_{fi}\sqrt{\mathrm{Re}_\xi},\ c_{fi} = \tau_i|_{\lambda=0}/(0.5\rho_\infty U_\infty^2)\ (i=1,2),$$
$$c_f^* = (c_{f_1}^{*2} + c_{f_2}^{*2} + 2c_{f_1}^* c_{f_2}^* \cos\psi)^{1/2},\ \mathrm{St}^* = \mathrm{St}\sqrt{\mathrm{Re}_\xi},$$
$$\mathrm{St} = q|_{\lambda=0}/(\rho_\infty U_\infty c_p (T_\infty - T_w))$$

(Re_ξ is the Reynolds number based on the incident stream parameters and the distance from the body vertex, and $\cos\psi = g_{12}/(g_{11}g_{22})^{1/2}$).

The computing algorithm provides for automatic rejection of regions of boundary layer separation in the vicinity of the plane of symmetry of the problem from the windward and the leeward sides [16].

3. The efficiency of the algorithm and the subroutine was checked on an example of determining the boundary layer on an elliptic cone [16].

The investigation of the three-dimension compressible boundary layer was accomplished on the surface of a sharp body of bielliptic cross section. The nose section with $\xi \leq 0.1$ is a circular cone with a semi-vertex angle of 15°. The upper half is a continuation of the cone, and the lower half is a body with transverse sections in the shape of semi-ellipses. The lower semi-axis of these ellipses a varies according to the law

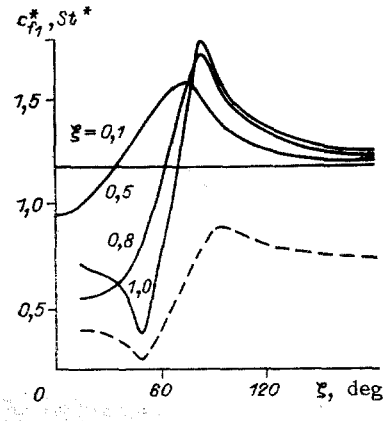

Fig. 2

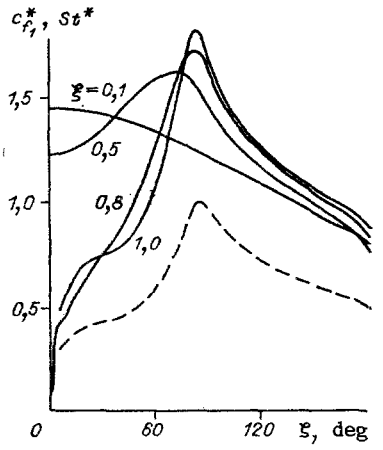

Fig. 3

$$a = \begin{cases} 0.26795\,\xi, & \xi \leqslant 0.1, \\ -0.55823\,\xi_1^3 + 0.26795\,\xi_1 + 0.026795, & \xi_1 = \xi - 0.1,\ 0.1 \leqslant \xi \leqslant 0.5, \\ 0.098248, & 0.5 \leqslant \xi \leqslant 1.0. \end{cases}$$

Hence, it can be seen that for $\xi = 0.1$ the lower generator has continuous first and second derivatives, and for $\xi = 0.5$ only the first derivative. The ratio of the semi-axes of the ellipse varies from 1 at $\xi \leq 0.1$ to 2.73 at $\xi = 1$.

To obtain the inviscid flow parameters we used a program described in [22]. The calculations were performed for $M_\infty = 2$ and $\alpha = 0$, 5, 10°. Figure 1 shows the static pressure distribution on the body surface as a function of the axial coordinate for $\zeta = 0$, 90, 180° and $\alpha = 10°$. On the conical nose the pressure does not vary with ξ, and in the transition section ($0.1 \leq \xi \leq 0.5$) it falls, and falls more sharply on the windward side. In the section where the lower generator is parallel to the axis ($\xi > 0.5$) the pressure increases, which can cause boundary layer separation in this region. If we draw the pressure distribution in the transverse section, we obtain the following picture. On the conical nose the maximum pressure occurs on the windward generator ($\zeta = 0$), and the transverse flow is parallel from the windward side to the leeward side. Later, as ξ increases the maximum pressure moves to a lateral position, which can lead to a change of direction of the transverse flow.

For $\alpha = 5°$ the nature of the pressure distribution is analogous to that described. For $\alpha = 0$ the maximum pressure is always located in the leeward plane of symmetry ($\zeta = 180°$), where the pressure practically does not vary. Its behavior as a function of ξ for $\zeta = 0$ is like that in the other two variants.

With the aid of the inviscid flow data for the above variants we computed the boundary layer for relative wall temperature $T_w = 1$. The number of rays in the layer was taken equal to 21 and 41. The same values were chosen for the number of nodes on a ray. The circumferential coordinate could be stretched, the step size in physical variables varying by a factor of 4.

Figures 2-4 show the distributions of $c_{f_1}^*$ in different cross sections for $\alpha = 0$, 5, 10°. The graphs show values of the coordinate ξ corresponding to each curve. For $\alpha = 0$ (see Fig. 2) on the conical nose ($\xi \leq 0.1$) the flow parameters do not depend on the circumferential coordinate ζ, and therefore c_{f_1} is constant. In the transition section $0.1 \leq \xi \leq 0.5$ on the windward side $c_{f_1}^*$ first increases, and then decreases. In the interval $0.5 \leq \xi \leq 1$ the pressure on the windward side increases and the flow decelerates in the boundary layer. At $\xi = 0.6$ flow separation occurs in the vicinity of the plane $\zeta = 0$. Later this region was excluded from the computation. The maximum of $c_{f_1}^*$ increased steadily and its location moved close to $\zeta = 83°$. On the leeward side $c_{f_1}^*$ varied only slightly.

In the variant described the plane $\zeta = 0$ is an inflow surface right up to the separation point. Then, due to the pressure increase the stream lines near the surface begin to move away from the plane of symmetry. This phenomenon is illustrated well in Fig. 5, which shows the distribution of $c_{f_2}^*$ in the section $\xi = 1$ for $\alpha = 0$, 5, 10°. It can be seen that for $\alpha = 0$ on the windward side the transverse overflows near the wall are positive, although

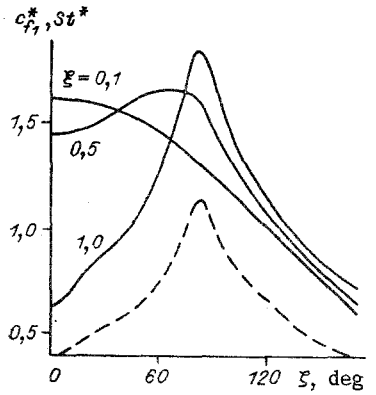

Fig. 4

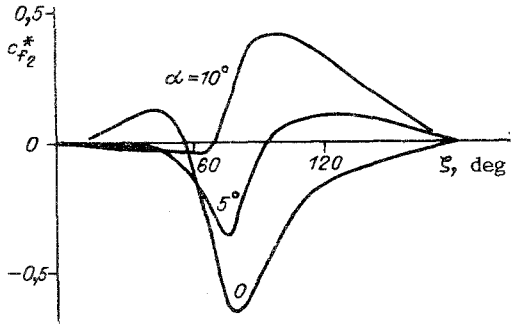

Fig. 5

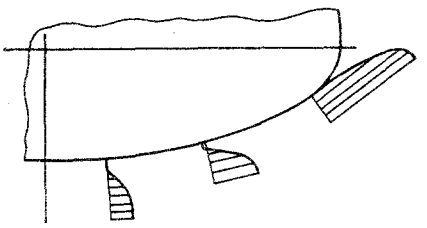

Fig. 6

at the outer edge of the boundary layer they are negative everywhere. Strictly speaking, here the perturbations from the left boundary $\zeta = 15°$ propagate within the computing region. But the angle between the stream lines and the coordinate lines is so small that the perturbations from the boundary can propagate along ζ to the end of the body through not more than 10°. In this variant the plane $\zeta = 180°$ is a divergent surface everywhere, except for the conical nose, where the flow is axisymmetric.

For $\alpha = 5°$ (see Fig. 3) on the conical nose $\xi \leq 0.1$ the value of $c_{f_1}^*$ is a maximum for $\zeta = 0$, where the outflow surface is located. In the transition section $0.1 \leq \xi \leq 0.5$ the maximum pressure is displaced to a lateral position, and behind it follows the maximum of $c_{f_1}^*$ with a delay. Here the transverse overflows near the wall for $\xi = 0.35$ change direction from positive to negative, and the outflow surface vanishes. In the section $0.5 \leq \xi \leq 1$ where the windward generator is parallel to the axis the pressure for $\zeta = 0$ increases, $c_{f_1}^*$ drops, and for $\xi = 0.9$ the boundary layer separates in a narrow region. The increase of pressure for $\zeta = 0$ produces a weak local maximum relative to ζ, and nevertheless the plane $\zeta = 0$ for $\xi \geq 0.7$ becomes an inflow surface, and the transverse overflows are parallel to the windward plane of symmetry in the region $0 \leq \zeta \leq 95°$ (see Fig. 5). The leeward plane of symmetry $\zeta = 180°$ in the variant is an inflow surface over the whole body length. The maximum of $c_{f_1}^*$ moves from the windward side to a lateral position, gradually increasing.

Beginning at a certain angle of attack, on the leeward generator of the sharp body one cannot construct a solution of the boundary layer equations with continuous derivatives in the transverse direction [15]. In our work the attempt to carry out the solution over the entire flow region led to the appearance of oscillations in ζ. To avoid these, the computing region for $\alpha = 10°$ (see Fig. 4) was restricted to the plane $\zeta = 170°$, through which the gas exits, and the boundary conditions of it were not applied. As can be seen from Fig. 4, the behavior of $c_{f_1}^*$ is analogous to that of the previous variant, the only difference being that the value $c_{f_1}^*$ in corresponding sections on the windward side is somewhat higher, and on the leeward side somewhat lower than for the case $\alpha = 5°$. Therefore $c_{f_1}^*$ for $\zeta = 0$ does not go to zero, i.e., separation does not occur. Regarding the outflow surface for $\zeta = 0$, it ends at the section $\xi = 0.5$. Later towards the end of the body the stream lines near the

body surface draw close to the plane of symmetry $\zeta = 0$, and move away from it near the outer edge of the boundary layer. This is illustrated in Fig. 6, which shows graphs for $\alpha = 10°$ of the transverse component of velocity w in the boundary layer on the windward and the lateral position of the body at the section $\xi = 1$.

We note, that the values of $c_{f_1}^*$ in the lateral position beyond the transition section are quite close for all three variants. For example, the difference of values at the point of maximum for $\xi = 0.5$ is 5%, and for $\xi = 1$ it is 3.5%. However, the position of this point is shifted a little to the windward side as the angle of attack increases.

The distribution of the similarity Stanton number St* is shown by a broken line in the latter section in Figs. 2-4. By comparing the curves of St* with those of $c_{f_1}^*$ for $\xi = 1$ one can see they are roughly similar. An analogous situation is observed also in the other sections. This phenomenon can be explained by the approximate validity for such complex flows of Reynolds analogy between heat transfer and friction [23].

The computed results have shown a significant influence of angle of attack on the flow picture in the boundary layer. With increase of α from 0 to 10° one observes the following qualitative changes. On the windward generator $\zeta = 180°$ the outflow plane transforms into an inflow plane. Although the character of the pressure distribution along the windward generator for these angles of attack is the same, the flow picture here changes substantially. The inflow surface with subsequent separation at $\xi = 0.6$ converts into an outflow surface in sections $\xi < 0.35$; $0.7 < \xi < 0.9$ for $\alpha = 5°$ and in the section $\xi < 0.5$ for $\alpha = 10°$. In the remaining sections in both variants the stream lines near the body move close to the plane $\zeta = 0$ and near the outer edge of the boundary layer they move away from it. Thus, there is no outflow surface in these regions.

The decrease of the radius of curvature in the transverse direction on the lateral position of the body causes an increase there of the similarity component of the friction factor $c_{f_1}^*$ at all angles of attack. On the windward side with increase of angle of attack it changes both qualitatively and quantitatively. With increase of α the transverse component $c_{f_2}^*$ increases from negative values to positive values everywhere, except for the windward side, where the changes are opposite in nature. For $\alpha = 5$ and 10° the maximum pressure is moved to the lateral position, and on the windward side a positive pressure gradient appears in the transverse direction, which turns around the flow near the wall towards the windward generator.

LITERATURE CITED

1. T. Cebeci, K. Kaups, and A. Moser, Calculation of three-dimensional boundary layers, III. Three-dimensional flows in orthogonal curvilinear coordinates, AIAA J., 14, No. 8 (1976); RTK, 14, No. 8 (1976).
2. H. A. Dwyer, Solution of a three-dimensional boundary layer flow with separation, AIAA J., Vol. 6, No. 7 (1968); RTK, 6, No. 7 (1968).
3. K. C. Wang, "Laminar boundary layer over a body at extremely high incidence," Phys. Fluids, 17, No. 7 (1974).
4. L. M. Vetlutskaya and V. N. Vetlutskii, "Computation of the three-dimensional incompressible laminar boundary layer on a flat plate with a step," ChMMSS, 11, No. 4 (1980).
5. Yu. D. Shevelev, "Numerical computation of a three-dimensional boundary layer in an incompressible fluid, Izv. Akad. Nauk SSSR, Mekh. Zhidk. Gaza, No. 5 (1966).
6. G. N. Andreev and Yu. D. Shevelev, "Three-dimensional boundary layer on a segmented body in supersonic flow," Izv. Akad. Nauk SSSR, Mekh. Zhidk. Gaza, No. 3 (1971).
7. I. D. Vvedenskaya, "Three-dimensional laminary boundary layer on a blunt body," Izv. Akad. Nauk SSSR, Mekh. Zhidk. Gaza, No. 5 (1966).
8. G. N. Andreev, A. K. Burdel'nyi, V. V. Minovtsev, and K. G. Savinov, "Investigation of three-dimensional flow over blunt bodies, accounting for viscosity on the basis of boundary layer theory," Nauch. Trudy Inst. Mekh., Mosk. Gos. Univ., No. 41 (1975).
9. R. M. Kendall, W. S. Bonnett, C. T. Nardo, and M. J. Abbett, "Computation procedure for three-dimensional boundary layers on aircraft and aerospace vehicles," II AIAA Computational Fluid Dynamics Conf., Hartford, Conn. (1975).
10. J. E. Harris and D. J. Morris, "Solution of the three-dimensional compressible laminar and turbulent boundary layer equations, with comparisons with experimental data," Proc. 4th Intern. Conf. Numerical Methods in Fluid Dynamics, S. I. Springer (1975).

11. W. J. Rainbird, "Turbulent boundary layer growth and separation on a yawed cone," AIAA J., 6, No. 12 (1968); RTK, 6, No. 12 (1968).
12. W. B. Sturek and L. B. Schiff, Numerical simulation of steady supersonic flow over spinning bodies of revolution, AIAA J., Vol. 20, No. 12 (1982).
13. D. S. Dolling and W. K. Gray, Experimental study of supersonic turbulent flow on a blunted axisymmetric body, AIAA J., 24, No. 5 (1986).
14. Yu. D. Shevelev, Three-Dimensional Problems of Laminar Boundary Layer Theory [in Russian], Nauka, Moscow (1977).
15. N. D. Vvedenskaya, "Computation of the boundary layer generated in flow over a cone at angle of attack," Zh. VMMF, 6, No. 2 (1966).
16. L. M. Vetlutskaya and V. N. Vetlutskii, "Computation of the three-dimensional compressible laminar boundary layer on a sharp body," ChMMSS, 17, No. 5 (1986).
17. K. C. Wang, "Determination of the zones of influence and dependence for the three-dimensional boundary layer equations," J. Fluid Mech., 48, No. 2 (1971).
18. V. N. Vetlutsky, "Laminar boundary layer on a flat plate with a rotating cylinder," Comp. Fluids, 9, No. 4 (1981).
19. C. H. Reinsch, Smoothing by Spline Functions, Numerische Mathematik (1967), Bd 10.
20. E. Krause, Comment on "Solution of a three-dimensional boundary layer flow with separation," AIAA J., 7, No. 3 (1969).
21. D. Schwamborn, Laminare Grenzschichten in der Nähe der Anlegelinie an Flügeln und flügelähnlichen Körpern mit Anstellung, BRD (1981), (Forschungsbericht, DFVLR, N 81-31).
22. M. K. Aukin and R. K. Tagirov, "Method of computing supersonic flow over a vehicle in the presence of air fences, wings, and fins," ChMMSS, 11, No. 6 (1980).
23. G. Schlichting, Boundary Layer Theory [Russian translation], Nauka, Moscow (1974).

TURBULENT INCOMPRESSIBLE FLUID FLOW IN A CHANNEL WITH UNILATERAL MASS TRANSFER

Sh. A. Ershin, U. K. Zhapbasbaev, T. B. Kozhakhmetov, and A. V. Smol'yaninov

UDC 532.542

The great practical value of channel flows with mass transfer through a porous wall evokes extensive interest [1-3]. If laminar flow analysis can rely on the solution of the exact equations of viscous fluid motion, then the turbulent motions most important in practical respects, are unfortunately not yet subject to a reliable theoretical analysis. Well-founded expectations are bestowed on modern turbulence models whose perfection may result in the possibility of a theoretical computational prediction of many complex turbulent flow modes. However, without a sufficient base of experimental data it is difficult to compute successful forward progress except success should be expected for an obligatory combination of empirical and analytical approaches to the problem. Such empirical material for flows in channels with smooth impermeable walls has been obtained in [4-7] and, for example, with rough walls in [8]. As regards flows in channels with mass transfer through the wall, then insofar as we know analogous investigations are still nonexistent. The present paper is a part of a general investigation of turbulent flow in a plane channel with mass transfer through porous walls.

1. The tests were performed on an apparatus that is a flat channel of width $2B = 0.45$ m and height $2H = 0.034$ m operating in the pressure mode. The fan had a soft connection with an air duct of about 20 m extent, from which air is delivered again through a soft connection to a receiving diffuser at the input of the stabilized channel section 140H in length. Therefore, the possibility is eliminated of transmission of mechanical vibrations from the fan and metal air duct to the apparatus. The metal diffusor is executed according to Vitoshinskii and is connected to the experimental apparatus through a system of networks and gratings. The stabilized channel section is fabricated from 0.03 m wood chip shavings

Alma-Ata. Translated from Zhurnal Prikladnoi Mekhaniki i Tekhnicheskoi Fiziki, No. 1, pp. 62-68, January-February, 1991. Original article submitted March 7, 1989; revision submitted September 29, 1989.

0021-8944/91/3201-0057$12.50